A Fully Implantable and Programmable Epidural Spinal Cord Stimulation System for Rats With Spinal Cord Injury

Guangwei Mao, Zhijun Zhou, Hao Su, Yaozhong Chen, Jianjun Zhang, Chiyuan Zhang, Zhigong Wang, *Senior Member, IEEE*, and Xiaoying Lü

***Abstract*— Epidural spinal cord stimulation (ESCS) is a potential treatment for the recovery of the motor function in spinal cord injury (SCI) patients. Since the mechanism of ESCS remains unclear, it is necessary to study the neurophysiological principles in animal experiments and standardize the clinical treatment. In this paper, an ESCS system is proposed for animal experimental study. The proposed system provides a fully implantable and programmable stimulating system for complete SCI rat model, along with a wireless charging power solution. The system is composed of an implantable pulse generator (IPG), a stimulating electrode, an external charging module and an Android application (APP) via a smartphone. The IPG has an area of 25 × 25 mm^2 and can output 8 channels of stimulating currents. Stimulating parameters, including amplitude, frequency, pulse width and sequence, can be programmed through the APP. The IPG was encapsulated with a zirconia ceramic shell and two-month implantable experiments were carried out in 5 rats with SCI. The main focus of the animal experiment was to show that the ESCS system could work stably in SCI rats. The IPG implanted *in vivo* can be charged through the external charging module *in vitro* without anesthetizing the rats. The stimulating electrode was implanted according to the distribution of ESCS motor function regions of rats and fixed on the vertebrae. The lower limb muscles of SCI rats can be activated effectively. The two-month SCI rats needed greater stimulating current intensity than the one-month SCI rats The results indicated that the stimulating system provides an effective and simplified tool for studying the ESCS application in motor function recovery for untethered animals.**

Manuscript received 22 May 2022; revised 27 October 2022 and 26 December 2022; accepted 3 January 2023. Date of publication 5 January 2023; date of current version 2 February 2023. This work was supported in part by the National Natural Science Foundation of China under Grant 61874024 and Grant 62004036, in part by the Opening Foundation of State Key Laboratory of Bioelectronics in Southeast University under SKlb2021-k09, and in part by the Fundamental Research Funds for the Central Universities. *(Corresponding authors: Zhigong Wang; Xiaoying Lü.)*

Guangwei Mao, Hao Su, Jianjun Zhang, and Xiaoying Lü are with the State Key Laboratory of Bioelectronics, Southeast University, Nanjing 210009, China (e-mail: luxy@seu.edu.cn).

Zhijun Zhou, Chiyuan Zhang, and Zhigong Wang are with the Institute of RF- and OE-ICs, Southeast University, Nanjing 210009, China (e-mail: zgwang@seu.edu.cn).

Yaozhong Chen is with the Zhongda Hospital, Southeast University, Nanjing 210009, China.

Digital Object Identifier 10.1109/TNSRE.2023.3234580

***Index Terms*— Epidural spinal cord stimulation, spinal cord injury, motor function recovery, electrode, implantable pulse generator.**

I. Introduction

SPINAL cord injury (SCI) is a severe trauma, with over 900000 new patients worldwide in 2016 [1]. SCI places a heavy burden on patients, families, and society. The treatment of SCI is still one of an unsolved medical problem across the world. The recovery of motor function has a high priority for patients with SCI [2].

Epidural spinal cord stimulation (ESCS) has been proven to be beneficial to the recovery of motor function in animal experiments and clinical experiments [3], [4], [5], [6], [7], [8], [9]. In ESCS, the stimulating electrodes are placed on the surface of the spinal dura below the injured site of the spinal cord. The electrical stimulation is applied to activate the undamaged neural network and promote motor function recovery [10], [11].

However, the neurophysiological mechanisms by which ESCS restores motor function after SCI are not completely clear [11], [12], [13].The recovery time and effect of motor function of SCI animal models and patients were varied and determined by the ESCS strategy among the completed ESCS studies [14]. ESCS treatments for restoring motor function are still in clinical trials. The recovery of motor function by ESCS also requires long-term and extensive rehabilitation training [15], [16], which may bring a heavy burden to the persons with SCI. Further long-term implantable experiments need to be carried out in SCI animal models to explore therapies with a better motor function recovery effect, a lower treatment cost with a higher safety, which can promote large-scale clinical trials [5] and meet the demands of more SCI patients.

The SCI rat model is often used as a common animal model to study the treatment methods and mechanisms of ESCS [17], [18], and a fully implantable ESCS system suitable for the SCI rat model is needed. The system should have the characteristics of small volume, long service life, multichannel and programmable stimulating parameters.

Although there have been some implantable stimulators used for the treatment of various nervous system diseases in

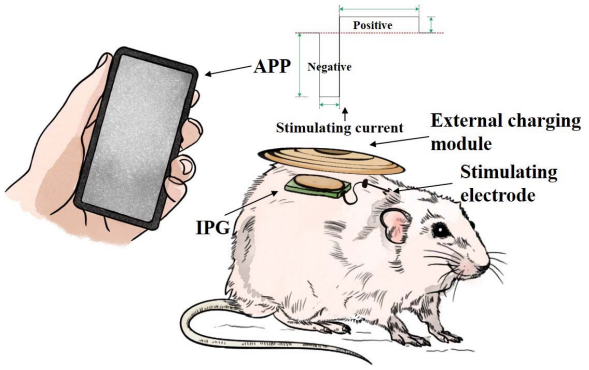

Fig. 1. Illustration of the stimulating system for ESCS.The IPG and stimulating electrode are implanted in the SCI rat. The researchers can use APP to program stimulation parameters. The external wireless charging module charges the lithium battery connected with IPG through the skin of rats. The IPG generates current stimulating signals to stimulate the spinal cord through the stimulating electrode. The rat can move freely during charging and stimulating.

clinical practice [19], these stimulators are not suitable for animal experiments, especially in small animal models such as rats, because of the large volume, high cost and the lack of secondary development interface. Some ESCS stimulators have been developed for animal experiments, but there are still some problems, such as incomplete implantation, few channels, and insufficient parameter range [20], [21], [22], [23], [24].

In this paper, a fully implantable and programmable ESCS system for the study of SCI animal models is introduced. The stimulating system is characterized by 8 channels, wireless charging and wireless programming stimulating parameters (stimulating amplitude, frequency, pulse width, channel and sequence). A platinum electrode array was designed according to the ESCS motor function regions of rats' lower limb muscles [25]. The IPG was encapsulated by a zirconia ceramic shell before implantable operation. The system is of small size, low cost and convenient to use. Two-month implantable animal experiments were carried out in 5 SCI rat models to verify the function of the ESCS system.

II. Materials and Methods

A. System Description

The stimulating system was shown schematically in Fig.1, including an IPG, stimulating electrodes, an APP via a smartphone, an external wireless charging module and a 150mah lithium battery (402525, zoncell, Shenzhen, China). The IPG was subcutaneously implanted in the backs of the rats. The stimulating electrode was implanted on the dural surface of spinal cord in the SCI rat. The external wireless charging module charges the lithium battery connected to the IPG through the skin of the rats.

The IPG generated current stimulating signals, which were transmitted to the spinal cord through a stimulation electrode, so as to activate the muscles of the rat lower limb. The APP can be used to program the stimulation amplitude, frequency, pulse width, channel, and sequence. After receiving the instructions

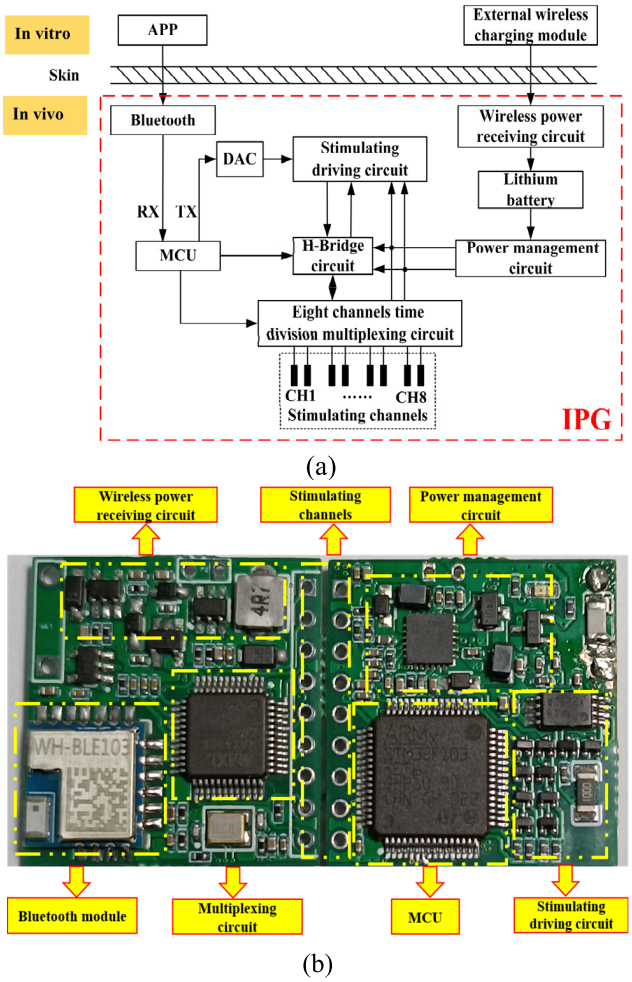

Fig. 2. Illustration of the IPG. (a) Block diagram of the IPG. (b) Circuit boards of the IPG. APP: Android application. DAC: digital to analog converter. IPG: implantable pulse generator. MCU: microcontroller unit.

sent by the APP, the IPG will generate asymmetric but charge balanced stimulating current showed in Fig. 1.

B. Implantable Pulse Generator

As shown in Fig. 2 (a) and (b), the IPG was composed of a microcontroller unit (MCU), a low-power Bluetooth communication module (BLE-103, USR, Jinan, China), a wireless power receiving circuit, a stimulating driving circuit, an H-bridge circuit, an 8-channel time division multiplexing circuit and a power management circuit. As presented in Fig. 2(b), the IPG circuit is made of four-layers of boards, with a size of $25 \times 25 \times 1.2$ mm^3.

The IPG had two modes: working and sleeping. The two modes can be converted by sending instructions through the APP. In the working mode, the circuit can generate current stimulation signals normally. In the sleeping mode, the MCU and the low-power Bluetooth module enter the sleeping state to reduce power consumption, extend the standby time, and reduce the charging time.

An STM32F103RET6 (ST, Geneva, Switzerland) was used as the microcontroller, processing the commands about stimulating parameters sent by the APP through the low-power

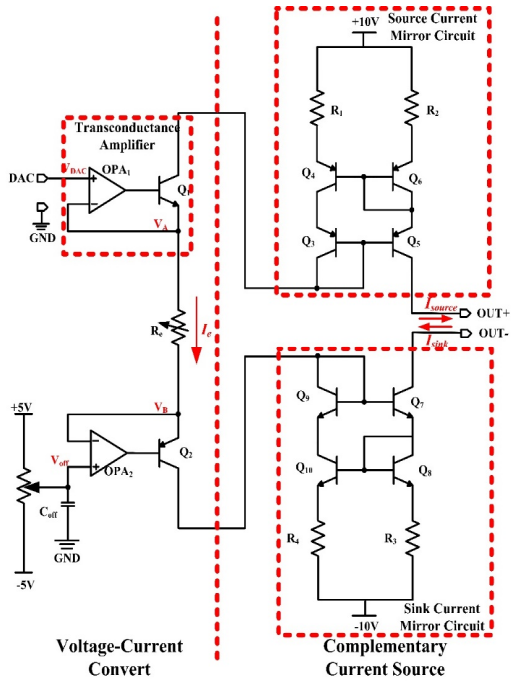

Fig. 3. The schematic diagram of the stimulating driving circuit in the IPG. DAC: digital to analog converter.OPA: operational amplifier.

Bluetooth communication module, then generating the needed voltage through the digital to analog converter (DAC) and outputting the initial signals to the stimulating driving circuit. The positive amplitude of the initial signals was set as 1/4 of the negative amplitude, and the pulse width was four times the pulse width of the negative. The stimulating driving circuit converted the voltage signals from the DAC into the constant current-stimulating signals, which pass through the H-bridge and 8-channel time division multiplexing circuit, so as to output the final stimulating current in the selected channels.

The power management circuit was used to provide power for each circuit in the IPG. The voltages required to supply the IPG mainly include mainly: 1) MCU supply voltage (3.3-V); 2) Bluetooth module supply voltage (3.3-V); 3) stimulating driving circuit and 8-channel time division multiplexing circuit supply voltage (±10-V)

A pair of improved complementary Wilson current mirrors [26] were used as the driving circuit of the IPG, in order to realize the linear conversion from voltage signals to current stimulating signals. The driving circuit schematic diagram, which was composed of a voltage-to-current converter and a complementary current source, is shown in Fig. 3.

The voltage-to-current converter included two coupled transconductance amplifiers, a series resistor and an amplifier offset-remove circuit, which could convert the voltage of the DAC into an accurate reference current (I_{ref}) to the complementary current source. Ideally, because of $V_{\mathrm{A}} = V_{\mathrm{DAC}}$ and $V_{\mathrm{B}} = 0$, I_{ref} can be calculated according to Eq. (1).

$$I_{\mathrm{ref}} \approx I_{\mathrm{e}} = \frac{V_{\mathrm{A}} - V_{\mathrm{B}}}{R_{\mathrm{e}}} = \frac{V_{\mathrm{DAC}}}{R_{\mathrm{e}}} \tag{1}$$

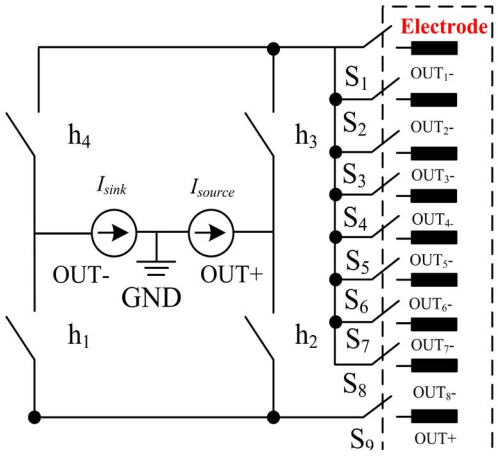

Fig. 4. The schematic diagram of H-Bridge circuit and 8-channels time division multiplexing circuit.

The complementary current source circuit consists of a source current mirror and a sink current mirror. The PNP transistors (Q3 ∼ Q6) and resistors (R1 and R2) form the source current mirror, and the NPN transistors (Q7 ∼ Q10) and resistors (R3 and R4) employ the sink current mirror. To reduce the circuit area, the transistors adopt the encapsulated by SC-89. The complementary current source can generate equivalent currents in opposite directions based on the Iref. The outputs of the two current mirrors (Isource and Isink) were connected to the H-bridge to generate biphasic pulses. As shown in Eq. (2), the Isource and Isink can be approximately estimated as:

$$I_{\mathrm{source}} = I_{\mathrm{sink}} \approx I_{\mathrm{ref}} \approx \frac{V_{DAC}}{R_e} \tag{2}$$

The H-bridge circuit and 8-channel time division multiplexing circuit were used to generate bidirectional, asymmetric and charge balanced current stimulating signals. The H-bridge circuit consisted of four analog switches and was connected to the output Isource and Isink of the complementary current source. By controlling the switches h_1 and h_2 through MCU, the negative and positive phase stimulating signals can be produced. The output of the H-bridge circuit is regarded as a single channel output. The 8-channel time division multiplexing circuit consists of eight analog switches, which were used to select the output channels among eight channels controlled by switches S_1 - S_8 through the MCU. The switches above were integrated into MAX4968 (Maxim, San Jose, USA). The MAX4968 communicates with the MCU based on the SPI protocol.

C. Wireless Power Transmission

The lithium battery implanted in rats could be charged through an external charging device. A schematic diagram of the external charging device and the wireless receiving circuit of the IPG based on the principle of electromagnetic induction is shown in Fig. 5 (a) and (b). The external charging module and the wireless receiving circuit used the XKT-801

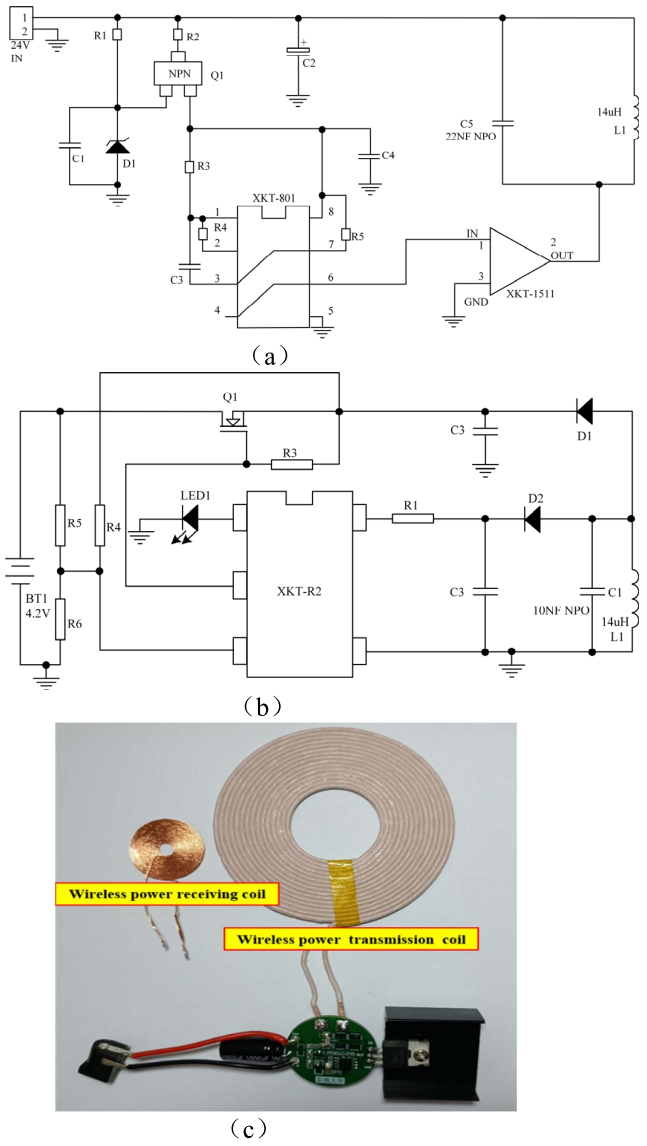

Fig. 5. Wireless power transmission circuit. (a) Schematic diagram of the wireless receiving circuit. (b) Schematic diagram of wireless transmitting circuit. (c) Wireless transmitting circuit and coils.

and XKT-R2 (XKT, Shenzhen, China) as the integrated power management chip respectively. XKT-801 is a high-frequency resonance high-power integrated circuit dedicated to long-distance charging. XKT-R2 has the functions of stabilization and reduction voltage, which can convert the input energy from the external charging module into a stable 4.2-V DC voltage for charging a lithium battery. As shown in Fig. 5 (c), the diameters of the transmitting and receiving coils (Guangcheng, Huizhou, China) are 80 mm and 25 mm, respectively and their inductance value is 14 μH. Although the large-diameter transmitting coil will reduce the charging efficiency, rats can move freely during charging without anesthesia or restraint.

D. Electrode Array

It was previously discovered that the lateral site of L1 and the medial site of L2 vertebrae segment of the spinal cord are the stimulation sites to activate the vastus lateralis (VL)

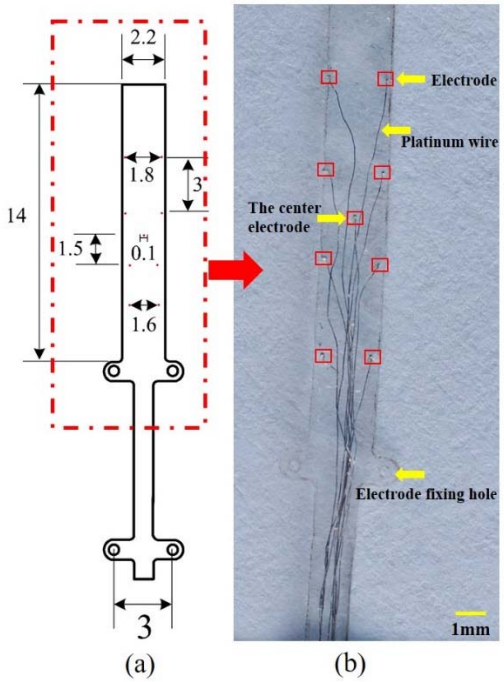

Fig. 6. Illustration of the stimulating electrode. The electrode array was made of silica gel and platinum wires. The electrode array has nine electrodes and leads. The diameter of the electrode point is 0.1 mm. The width of the stimulating electrode is 2.2 mm, the length is 14 mm, and the thickness is 0.1 mm. (a) The size of the stimulating electrode(mm). (b) The stimulating electrode.

and gastrocnemius (MG) in previous studies [18], [25]. According to the distribution of stimulation sites in rats, the electrode array shown in Fig. 6 was designed. The array was implanted into the spinal cord of L1-L2 segments of the SCI rat vertebrae. The electrode array had nine electrodes and leads. The diameter of the electrode point is 0.1 mm. Four electrical points in the head of the electrode array were used to stimulate VL, and four electrical points in the tail of the electrode array were used to stimulate the MG. Four symmetrical electrode fixing holes were designed to anchor the stimulating electrodes in vivo and let the electrode attach onto the dura mater of the spinal cord closely. The width of the stimulating electrode was 2.2 mm, the length was 14 mm, and the thickness was 0.1 mm. The anode was set as the center point of the stimulating electrode. As shown in Fig. 6(b), the electrode substrate was made of silica gel, and the electrode leads were made of platinum wires. The platinum wire was wrapped with silica gel and formed at 120 °C in a mold (KEDOUBC, Suzhou, China). A precision impedance analyzer (IM3536, HIOKI, Kagoshima, Japan) was used to measure the impedance of the stimulating electrode from 10 Hz to 1 kHz in in normal (0.9%) saline before the implantation.

E. Android APP

The user interface of the Android APP is shown in Fig. 7. The APP was developed based on the Android studio (Google, San Francisco, CA, USA) platform to control the IPG. The APP realizes the conversion of IPG in working and sleeping

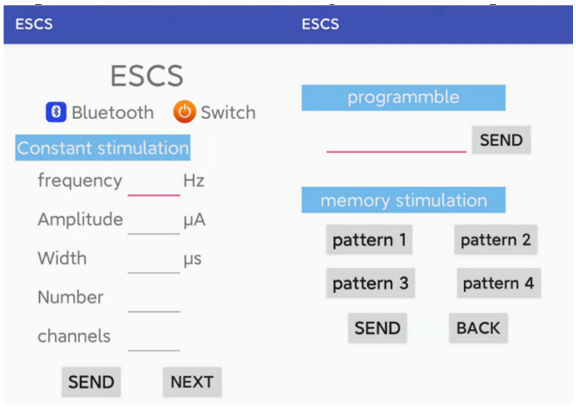

Fig. 7. Screenshot of the Android APP interface.

modes by sending instructions. In the working mode, the APP sends the stimulating parameters to the IPG via a Bluetooth module. The MCU analyzed the stimulating parameters, generated the stimulating signals, and selected the stimulating channels. The Android APP was designed with 3 stimulating models: 1) The constant stimulation for user inputting, which outputs stimulating signals by directly inputting stimulating parameters in the input box; 2) The programming stimulation by inputting continuous instructions about stimulating parameters; and 3) The memory stimulation can save and call commonly used programming stimulating instructions.

F. IPG Encapsulation

The part implanted in SCI rats of the stimulating system included an IPG, a lithium battery, a wireless power receiving coil and a stimulating electrode, as shown in Fig.8(a).

Zirconia ceramics, which have a high temperature resistance and a good biocompatibility and has been used in rechargeable implantable stimulation devices [19], was used as the encapsulation material. As shown in Fig. 8(b), a 3 × 3 × 1-cm^3 zirconia box (YAMEI Dental, Nanjing, China) was designed according to the size of the IPG. The IPG was placed inside the box, and the electrode array was protruded out of the box through a small hole in the box. The box was cemented using resin cement (Pulpdent, Watertown, USA). Finally, the box was bonded to a slice of polyethylene mesh (Hualikang, Nantong, China) with resin cement. The polyethylene mesh could be fixed to the rat back muscles by surgical sutures to prevent displacement of the IPG during the *in vivo* experiments.

G. The Key Parameters of the Stimulation System

The resistance value of R_e in Eq. (2) cannot be too small; otherwise, the IPG will overheat because of the large current generated from the driving circuit. In this study, the resistance value of R_e was 100 Ω. The output current of the IPG could be adjusted from 1 μA to 10 mA with a minimal resolution of 1 μA when the output impedance was less than 1 kΩ. The stimulating frequency varied between 1-1000 Hz in 1-Hz increments. The range of pulse width was 0-2000 μs, and the minimum resolution was 5 μs. Table I showed the key parameters of the stimulation system designed in this study.

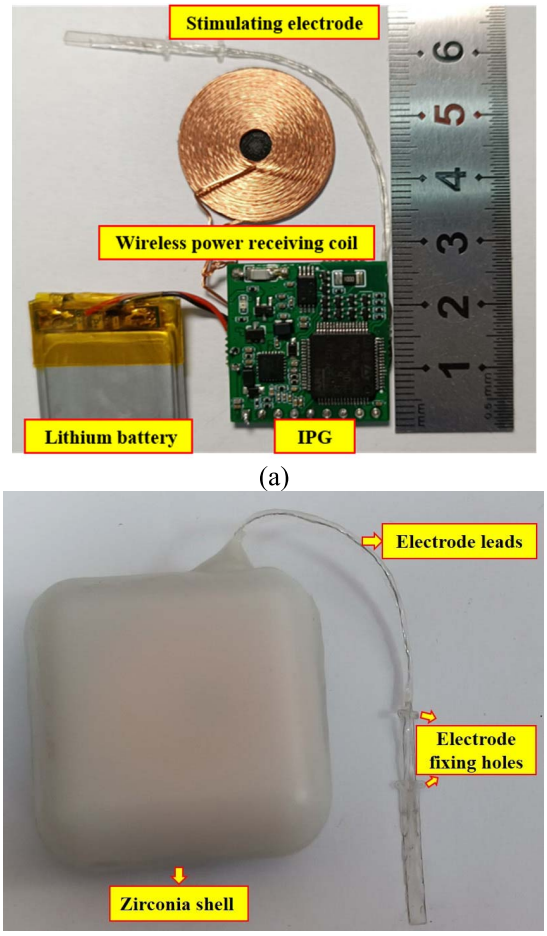

Fig. 8. Illustration of the IPG Encapsulation. (a) The part implanted in SCI rats of the stimulating system. (b) The IPG encapsulated with a zirconia shell.

TABLE I
KEY PARAMETERS OF THE STIMULATING SYSTEM OF ESCS

Parameters	Value(Resolution)
number of channels	8
output characteristic	constant current
waveform type	biphasic, square wave
pulse amplitude	0-10 mA(1 μA increment)
pulse frequency	0-1000 Hz(1 Hz increment)
pulse width	0-2000 μs (5μs increment)
current consumption in working mode	58 mA
current consumption in sleeping mode	8 mA
weight of IPG	8.4 g
weight of IPG with zirconia ceramics	35 g
electrode material	platinum

H. Operation

Five specific-pathogen-free female Sprague-Dawley rats weighing 180-200 g and aged 7-8 weeks were provided by

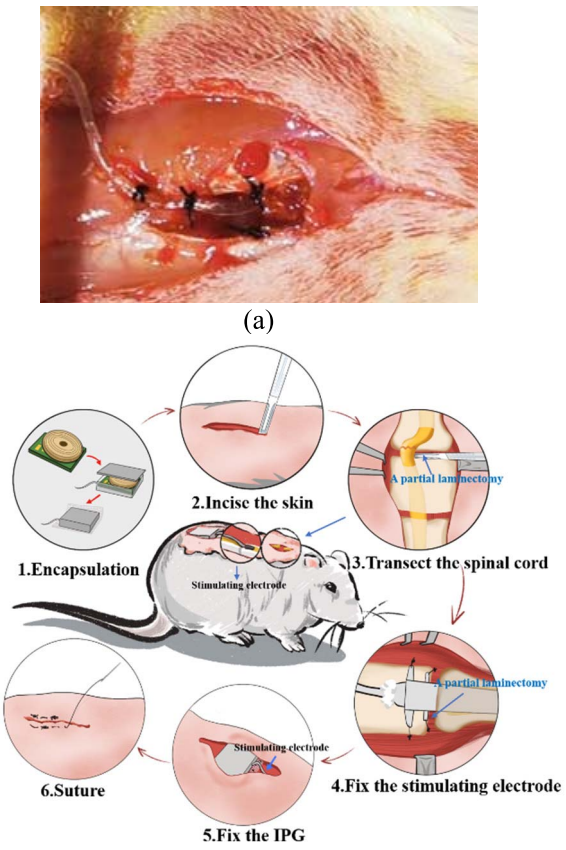

Fig. 9. Illustration of the operation. (a) The suture of the electrode array. (b) The deconstructed parts of the stimulation system that are implanted in the SCI rats.

Zhejiang Experimental Animal Center, China [license No. SCXK (Zhe) 2019-0002]. All experimental processes mentioned below complied with the Guidelines for the Care and Use of Laboratory Animals of the US National Institutes of Health [27], and all surgical operations were performed under sterile conditions.

The rats were anesthetized by isoflurane gas (RWD, Shenzhen, China) on a heating pad (Xinong, Beijing, China). A partial laminectomy was performed at T10 vertebrae of the rats to expose the spinal cord, and a section of spinal cord (approximately 2 mm) was removed with an ophthalmic scissors. The incision was plugged with a hemostatic sponge(CARENT, Zhejiang, China) [28]. Then, the spinous process of the L2–L3 vertebrae were removed to insert the stimulating electrode through the space between the L2–L3 vertebrae. The stimulation signals with a pulse width of 200 μs, a current strength of 400 μA, and a frequency of 1 Hz were applied to adjust the position of the electrode by observing and touching the lower limb muscles, and ensure that the stimulating electrode could activate the MG and VL of both lower limbs.

After determining the position of the stimulating electrode, the electrode fixing holes of the electrode were sutured by polyamide suture (3-0, Yuanlikang, Jiangsu, China) with the paravertebral muscles as shown in Fig. 9(a), and the leads of the electrode were fixed on the vertebra by dental cement(ShangChi, Shanghai, china) and closure clip (Prader, Jiangsu, China). The array was fixed with dura by polyamide suture (5-0, Yuanlikang, Jiangsu, China). The leads were fixed with the the paravertebral muscles by polyamide suture (3-0, Yuanlikang, Jiangsu, China). Then, the zirconia box bonded with polypropylene mesh was implanted subcutaneously into the backs of rats, and the polypropylene mesh was fixed on the back muscles with polyester sutures (3-0, Yuanlikang, Jiangsu, China). Finally, the back skin was sutured by tension-reducing suturing with polyester sutures (0-0, Yuanlikang, Jiangsu, China). All steps of the operation are shown in Fig. 9(b).

The rats implanted with IPG were kept separately in their own incubators and given sufficient food and water, and the corncob padding was changed every five days. The rats were given 10 mg of amoxicillin (McLean, Shanghai, China) and the wounds on the skin surface of the rats were wiped with iodine every day to prevent infection. In the first two days, rats were given 5 mg of ibuprofen(Renhe, Fujian, China). The bladders of the rats were massaged and the urethral orifice was cleaned with alcohol cotton four times a day. The rats recovered 7-10 days after implantation. During the recovery, the implantable pulse generator in rats was charged with an external charger for 15 minutes every day. The state of the wireless charging can be confirmed by the LED light of the IPG.

I. Recording of the Electromyography Signals

Electromyography (EMG) signals were to evaluate of ESCS with different stimulating parameters. EMG signals of rats were detected one month and two months after implantation. The reference electrode was placed on the exposed skin on the back of the rat. The rats were anesthetized with isoflurane gas during EMG signal recording. Disposable concentric needle electrodes (NEC2530, Friendship medical, Shanxi, China) were inserted into the lower limb muscles of rats, which were connected with a multichannel physiological signal amplifier (A-M Systems, Sequim, USA) to record the EMG signals. The gain was set to 1000 to amplify the EMG signals and the passband of EMG filtering was 10–1000 Hz. The EMG signals were sampled at 10 kHz, and saved using a 16-channel Power Lab data-acquisition system (AD Instruments, New South Wales,Australia). The root mean square (RMS) values of the stimulating responses were used to evaluate the effect of ESCS. The data are expressed as the mean±standard deviation(SD). The current thresholds for activating the different muscles were recorded. The significance in the current thresholds was analyzed using a paired Student's t-test. A value of $P < 0.05$ was considered statistically significant.

III. Results

A. In Vitro Functional Test

The impedances of electrode arrays across a range of frequencies are shown in the Fig. 10. The impedance was found to be 168.6 ± 38.9 kΩ in normal (0.9%) saline at 100 Hz.A power analyzer (UTA0601, Toomss, Chongqing, China) was used to measure the current consumption of

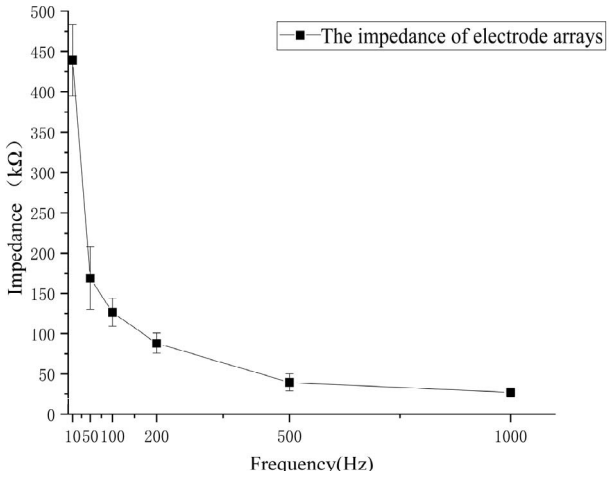

Fig. 10. The impedances of electrode arrays. The data are expressed as the mean ± standard deviation.

the IPG. The current consumption in the working mode and sleeping mode of the IPG was 58 mA and 8 mA, respectively. The IPG can work normally for approximately two hours with a 150-mAh lithium battery. The power consumption of the sleeping mode is 86% lower than the power consumption of the working mode, and the standby time of the implantable stimulator is prolonged. The receiving current of the IPG was measured with a pointer ammeter (85C1, Elecall, Wenzhou, China), and the external charging module charged the lithium battery of the IPG across the zirconia ceramic with a distance of 1.5 cm. The charging current was 420 mA, and the 150-mAh lithium battery could be fully charged in approximately 20 minutes.

The output current of the IPGs was measured before the implantation. Fig. 11(a) showed the relationship between ideal and measured output current amplitudes of the five IPGs with the 1-kΩ load impedance. The power supply of the driving circuit was ±10 V and the maximum output current were 10 mA. The linearity and maximum output current was limited by the power rails. Therefore, the measured output current gradually deviated from the ideal curve and was lower than the ideal output current amplitudes. The spinal cord impedance of experimental animals is usually less than 1 kΩ [28], and the IPG can provide sufficient stimulation strength. As shown in Figure 11(b), a stimulating signal of the IPG with the 1-kΩ load impedance was recorded by the Power Lab data-acquisition system (AD Instruments, Australia). The negative stimulating waveform with pulse width of 200 μs and amplitude of 1mA was set through APP.

B. Animal Experiment Test

As shown in Fig. 12, the wounds of the rats implanted with IPG healed completely after the operation. During the two-month experimental period, we charged and stimulated the IPG implanted in rats every day to test whether the IPG worked normally. The 8-channel stimulating signals were applied in turn through the stimulating electrode, which can activate the

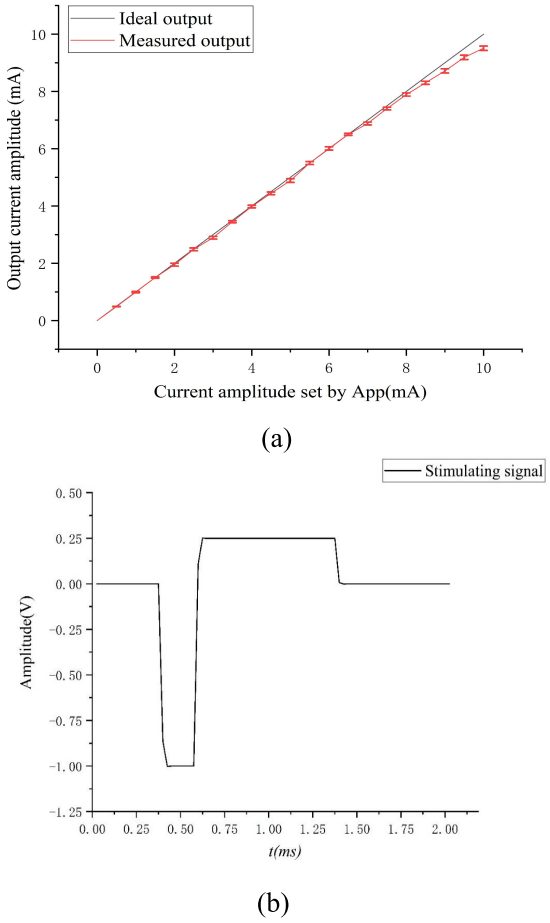

Fig. 11. Output current test of the IPGs in vitro. (a) The relationship between ideal and measured output current amplitudes of the five IPGs with the 1k¯ load impedance. The data are expressed as the mean ± standard deviation. (b) A Stimulating signal of the IPG. The negative stimulating waveform with pulse width of 200 μs and amplitude of 1 mA.

gastrocnemius muscles, vastus lateralis(VL) consistent with the distribution of ESCS motor function regions [18], [25].

First, the current thresholds of the limb muscles of the activating rats were recorded. The single stimulating current pulse was increased or decreased with a step size of 10 μA to determine the thresholds of MG and VL. As shown in Fig. 13(a), the thresholds of MG and VL between the one-month and two-month-old rats were significantly different ($P < 0.01$). The two-month SCI rats need greater stimulating current strength than the one-month SCI rats.

The stimulating current with 0.2 Hz, and 200 μs was used to activate left VL by stimulating the same electrode point in five SCI rats at one month and two months after implantation, and the stimulating responses were recorded and analyzed. The RMS of stimulating responses was calculated as Eq. (3):

$$RMS_{EMG} = \sqrt{\frac{\sum_{i=0}^{N} x_i^2}{N}} \tag{3}$$

where N is the number of recording points and x_i is the value of the stimulating responses. Ten stimulating responses were recorded for each stimulating current of five SCI rats.

(a)

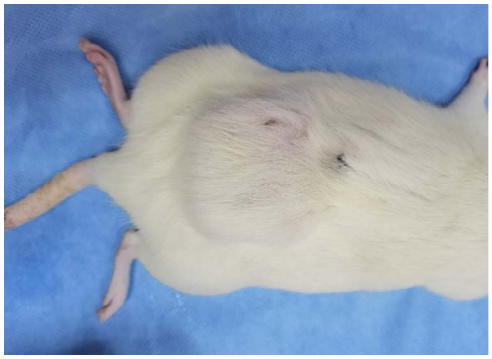

(b)

Fig. 12. The rat implanted with IPG. (a) The zirconia shell with IPG was implanted in the rat during operation.(b) The wound of the rat healed in seven weeks after operation.

The relationship between stimulating responses and stimulating current of VL of one-month and two-months rats were shown in Fig. 13 (b) and (c), respectively. The strength of stimulating responses was enhanced with the increase of stimulating amplitude, which verified the effectiveness of the IPG *in vivo*.

Fig. 13(d) showed a typical example of a rat's stimulating responses in left MG with a stimulating amplitude of 600 μA, a pulse width of 200 μs and a frequency of 100 Hz. The frequency of stimulating responses was consistent with stimulating signals.

IV. Discussion

This paper proposes an 8-channel fully implantable and programmable current stimulating system with wireless charging suitable for ESCS in SCI animal models. The system consists of an IPG, a stimulating electrode array, an external charging module and an Android application (APP) via a smartphone. Commercial discrete electronic components are used in this system, which have the characteristics of low cost. The stability and effectiveness of the ESCS system was confirmed by a two-month implantable experiment in five SCI rats.

The required stimulating intensity for ESCS to activate motor activity in rats varies at different time points after SCI [29], [30]. This study also found that two-month SCI

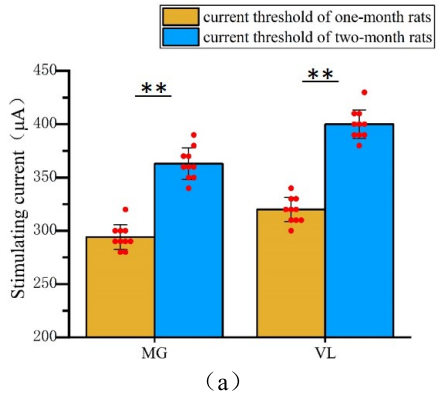

（a）

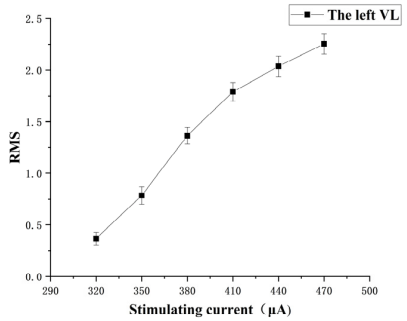

(b)

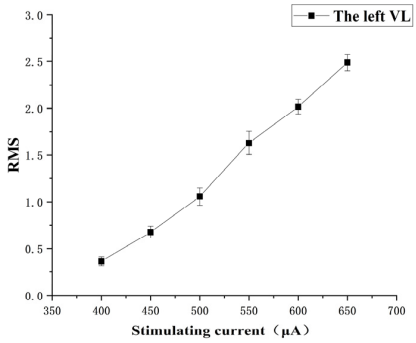

(c)

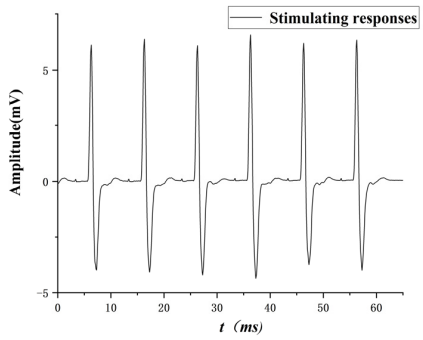

(d)

Fig. 13. The stimulating responses. (a) The current threshold of SCI rats at one-month and two-month. The data are expressed as the mean ± standard deviation(n = 5).There was a significant difference between the thresholds of the VL and MG at one-month and two month. (Student's t-test; **P < 0.01)) (b) The relationship between stimulating current and responses of VL at one-month after implantation. (c) The relationship between stimulating current and responses of VL at two-month after implantation. (d) The stimulating responses in MG of a rat with a stimulating amplitude of 600uA, a pulse width of 200μs and a frequency of 100Hz. VL: vastus lateralis.MG: gastrocnemius.

TABLE II
A SUMMARY OF COMPARISONS OF THE STIMULATING SYSTEM

	Zhou(2012) [20]	Xu (2015) [21]	Gudrun(2018) [22]	Chen (2020) [23]	Hogan(2020) [24]	This work
Channels	1	2	1	1	8	8
Programmable	Yes	Yes	Yes	Yes	Yes	Yes
Waveform type	biphasic	monophase	monophase	monophase	biphasic	biphasic
Pulse amplitude	0.1-10V	50 mV-3V	10μA-1mA	2V-8V	0-5 mA	0-10 mA
Communication	MSK	ASK	\	BLE	RF @2.4GHz	BLE
Size of IPG(cm^2)	7.92	5.06	13.5	4	\	6.25
Encapsulation	silicone	silicone	\	PDMS	epoxy	zirconia

rats need greater stimulating current strength than one-month SCI rats [25], [29]. Moreover, the amplitude, frequency and sequence of ESCS are important for the recovery of motor function [14]. It is necessary to constantly optimize the stimulation parameters during treatment. The stimulator also needs to have the abilities of convenient programming and a wide range of stimulation parameters. In our study, the amplitude, frequency, pulse width, stimulating channel and sequence of stimulating signals provided by the IPG can be conveniently programed by the APP, and the sufficient range and the fine regulation of stimulating parameters meet the requirements for experiments. The stimulating system designed in this study also has the function of wireless charging. During charging, the light emitted by the light-emitting diode in the wireless power receiving circuit of the IPG can be seen through the back skin of rats, so as to judge whether the charging function is in order. The IPG in rats can be charged safely and conveniently, because the diameter of the charging coil used in the system reaches 8 cm. Stimulators without batteries can reduce the volume of stimulators and the risk of battery leakage [20], [23]. However, they need external controllers to supply power to the stimulators all the time, which is inconvenient for the free movement and rehabilitation training of animal models.

The purpose of implanting stimulating system for SCI rats is to restore the motor function. It is necessary to study stimulating strategies in different motion scenes, such as treadmills. The working time of the IPG after charging fully meets a rehabilitation training session. The parameters of 8-channel stimulating signals can be programmed arbitrarily and satisfy the premise of stimulating strategies research. The stimulating system designed in this paper may also be used in the study of neuromodulation in other diseases and animal models. The amplitude of stimulating signals provided by the IPG can meet the requirement in larger SCI animal models, such as pig [31] and monkey [8]. If a higher stimulating amplitude is needed, it is only necessary to increase the power supply voltage of the driving circuit of the IPG to output higher intensity current signals.

To achieve the success of long-term implantable animal experiments, two main problems need to be solved: the encapsulation of implants and the dislocation of the stimulating electrodes. First, we chose zirconia ceramics and resin cement as encapsulation materials. Compared with common polymer encapsulation materials used in animal experiments [32], such as Polydimethylsiloxane, zirconia ceramics are widely used in stomatology and have a better biocompatibility [33]. Compared with titanium used in the clinic, zirconia ceramics can be used as a medium for wireless charging. Zirconia ceramics are the key to the application of wireless charging implants in primate models and patients. However, the encapsulation of zirconia ceramics was slightly heavier than the encapsulation of resin materials, which may make it difficult to restore the motor function of SCI rats. Further work is needed to reduce the size and quality of the zirconia shell. Second, we designed a stimulating electrode array according to the distribution of stimulation sites in rats, which can be better positioned and fixed than wire stimulation electrodes [34]. In addition to using sutures to fix the electrode, dental cement was also used to fix the electrode on the vertebrae. The cement can fill the gap between vertebrae and fix the electrode. The electrode leads were fixed with a vascular clamp and suture to prevent the electrode array from shifting due to the movement of the electrode leads. Fixing the IPG with polyethylene mesh can not only prevent the stimulator from moving in rats, but also prevent the electrode from falling off due to the movement of the IPG.

Table II sums up the main attributes of the proposed system and other stimulators for animal experiments. The proposed system has advantages in the number of channels and the range of stimulating parameters. Compared with clinical stimulators used for the treatment of various nervous system diseases [19], the proposed system has a small volume, low cost, and secondary development interface. The fully implantable and programmable stimulator provided an efficient and convenient method that can be used in animal experiments for the treatment of various neurological diseases. For future clinical applications, our laboratory is focusing on the following two aspects: (1) We are researching the treatments of nervous system diseases by animal experiments [35]. (2) We are designing the stimulating chip to increase the number of channels, reduce power consumption, reduce the size of the IPG and prolong the working time [36].

Nerve stimulators can be divided into voltage stimulators and current stimulators. Although both types stimulators can output stimulating signals and activate nerve tissue effectively, they have their own advantages and disadvantages. Compared with voltage stimulators, the current stimulator consumes more energy because of the compliance voltage. However, the main advantage of the current stimulators is controlling

current injection directly. The electrical current is the prime determinant of neuronal responses. If the compliance voltage provided by current stimulators is sufficient, the current stimulating signals will not drift, which is appropriate for the fine adjustment of neuromodulation and consistent activation of neurons. In voltage stimulators, due to the charging of electrode capacitance, the stimulating current attenuates in the cathode phase and the waveform of the pulse is easily distorted. In addition, unpredictable or uncontrolled changes in impedance can affect the intensity of the stimulating current and may lead to unexpected safety problems, so it is difficult to accurately and safely control the activation of nerve tissue by voltage stimulation [19]. In the recovery of motor function by ESCS, a fine control is required [18], [25]. Therefore, the design of current stimulators was selected in this study.

Our research group has proposed a novel method to reconstruct motor functions using a microelectronic neural bridge (MENB) [37], [38], [39]. A MENB consists of a detecting module and a stimulating module. The detecting module processes the spontaneous neural signals from the spinal cord above the injured site, and then the stimulating module regenerates the stimulating signals, which are used to stimulate spinal cord below the injured site, so that the neural function of the injured spinal cord can be rebuilt. Thus, an MENB system acts as a multiple point-to-point relay and as a neural-function rebuilder [40]. The stimulating system proposed in this study can be used directly as the stimulating module of the MENB. The Bluetooth communication module of the IPG can directly communicate with the detecting module or other control module with Bluetooth, so as to receive neural signals from the spinal cord or control instructions including stimulating parameters. The MCU of the IPG also has sufficient processing power to process and analyze nerve signals, so as to form a closed-loop stimulating system.

Several limitations should be noted regarding this study. First, although the design of time division multiplexing can reduce the size of the IPG, the parameters of stimulating signals generated simultaneously by different channels are identical. Second, the power consumption of an IPG using discrete components is relatively high compared with an integrated circuit chip, and it is difficult to further increase the number of stimulating channels due to the limitation of the IPG size. Finally, the stimulating anode is fixed, which reduces the combinations of stimulating sites. These problems will be considered in the design of stimulating CMOS chip in the next step.

V. Conclusion

In this study, a novel multichannel, low-cost ESCS system with wireless charging and programming for SCI rats was developed, and the function of the ESCS system was verified by the two-month fully implantable animal experiments. The system included an IPG, a stimulating electrode, an external charging module and an Android application(APP) via a smartphone. The system can generate 8-channel bidirectional charge balanced stimulating signals. The stimulating channel, amplitude, pulse width, frequency and sequence can be programmed through APP. The IPG was encapsulated in zirconia and implanted subcutaneously in rats and the size of the implant was $3 \times 3 \times 1$ cm^3. Future work should focus on optimizing stimulating strategies for the ESCS therapy in SCI animal models implanted with the ESCS system.

References

[1] S. L. James et al., "Global, regional, and national burden of traumatic brain injury and spinal cord injury, 1990–201: A systematic analysis for the global burden of disease study 2016," *Lancet Neurol.*, vol. 18, no. 1, pp. 56–87, Jan. 2019.

[2] K. D. Anderson, "Targeting recovery: Priorities of the spinal cord-injured population," *J. Neurotrauma*, vol. 21, no. 10, pp. 1371–1383, Oct. 2004.

[3] A. W. Cook and S. P. Weinstein, "Chronic dorsal column stimulation in multiple sclerosis. Preliminary report," *New York State J. Med.*, vol. 73, no. 24, pp. 2868–2872, 1973.

[4] S. Harkema et al., "Effect of epidural stimulation of the lumbosacral spinal cord on voluntary movement, standing, and assisted stepping after motor complete paraplegia: A case study," *Lancet*, vol. 377, no. 9781, pp. 1938–1947, 2011.

[5] S. Wang, L. C. Zhang, H. T. Fu, J. H. Deng, and P. F. Tang, "Epidural electrical stimulation effectively restores locomotion function in rats with complete spinal cord injury," *Neural Regener. Res.*, vol. 16, no. 3, p. 573, 2021.

[6] F. B. Wagner et al., "Targeted neurotechnology restores walking in humans with spinal cord injury," *Nature*, vol. 563, no. 7729, pp. 65–71, Nov. 2018.

[7] M. L. Gill et al., "Neuromodulation of lumbosacral spinal networks enables independent stepping after complete paraplegia," *Nature Med.*, vol. 24, no. 11, pp. 1677–1682, 2018.

[8] M. Capogrosso et al., "A brain-spine interface alleviating gait deficits after spinal cord injury in primates," *Nature*, vol. 539, no. 7628, pp. 284–288, Nov. 2016.

[9] A. S. Gorgey and J. J. Gouda, "Single lead epidural spinal cord stimulation targeted trunk control and standing in complete paraplegia," *J. Clin. Med.*, vol. 11, no. 17, p. 5120, 2022.

[10] J. Holsheimer, "Which neuronal elements are activated directly by spinal cord stimulation," *Neuromodulation*, vol. 5, no. 1, pp. 25–31, Jan. 2002.

[11] J. T. Hachmann, A. Yousak, J. J. Wallner, P. N. Gad, V. R. Edgerton, and A. S. Gorgey, "Epidural spinal cord stimulation as an intervention for motor recovery after motor complete spinal cord injury," *J. Neurophysiol.*, vol. 126, no. 6, pp. 1843–1859, Dec. 2021.

[12] M. Capogrosso et al., "A computational model for epidural electrical stimulation of spinal sensorimotor circuits," *J. Neurosci.*, vol. 33, no. 49, pp. 19326–19340, Dec. 2013.

[13] E. M. Moraud et al., "Mechanisms underlying the neuromodulation of spinal circuits for correcting gait and balance deficits after spinal cord injury," *Neuron*, vol. 89, no. 4, pp. 814–828, Feb. 2016.

[14] E. Formento et al., "Electrical spinal cord stimulation must preserve proprioception to enable locomotion in humans with spinal cord injury," *Nature Neurosci.*, vol. 21, no. 12, pp. 1728–1741, Dec. 2018.

[15] E. Choi et al., "Epidural electrical stimulation for spinal cord injury," *Neural Regener. Res., Rev.*, vol. 16, no. 12, pp. 2367–2375, Dec. 2021.

[16] A. Rowald et al., "Activity-dependent spinal cord neuromodulation rapidly restores trunk and leg motor functions after complete paralysis," *Nature Med.*, vol. 28, no. 2, pp. 260–271, Jul. 2022.

[17] I. Lavrov et al., "Epidural stimulation induced modulation of spinal locomotor networks in adult spinal rats," *J. Neurosci.*, vol. 28, no. 23, pp. 6022–6029, Jun. 2008.

[18] P. Gad et al., "Development of a multi-electrode array for spinal cord epidural stimulation to facilitate stepping and standing after a complete spinal cord injury in adult rats," *J. NeuroEng. Rehabil.*, vol. 10, no. 1, p. 2, Jan. 2013.

[19] P. H. Peckham and D. M. Ackermann, "Implantable neural stimulators," in *Neuromodulation*, E. S. Krames, P. H. Peckham, and A. R. Rezai, Eds. New York, NY, USA: Academic, 2018, pp. 275–287.

[20] H. Zhou, Q. Xu, J. He, H. Ren, H. Zhou, and K. Zheng, "A fully implanted programmable stimulator based on wireless communication for epidural spinal cord stimulation in rats," *J. Neurosci. Methods*, vol. 204, no. 2, pp. 341–348, Mar. 2012.

[21] Q. Xu, D. Hu, B. Duan, and J. He, "A fully implantable stimulator with wireless power and data transmission for experimental investigation of epidural spinal cord stimulation," *IEEE Trans. Neural Syst. Rehabil. Eng.*, vol. 23, no. 4, pp. 683–692, Jul. 2015.

[22] G. E. Olafsdottir, W. A. Serdijn, and V. Giagka, "An energy-efficient, inexpensive, spinal cord stimulator with adaptive voltage compliance for freely moving rats," in *Proc. 40th Annu. Int. Conf. IEEE Eng. Med. Biol. Soc. (EMBC)*, Jul. 2018, pp. 2937–2940.

[23] X. W. Chen et al., "Design and experimental research of implantable lower esophageal sphincter stimulator based on Android Bluetooth," in *Proc. 42nd Annu. Int. Conf. IEEE Eng. Med. Biol. Soc. (EMBC)*, Jul. 2020, pp. 5220–5223.

[24] M. K. Hogan et al., "A wireless spinal stimulation system for ventral activation of the rat cervical spinal cord," *Sci. Rep.*, vol. 11, no. 1, p. 14900, Jul. 2021.

[25] G. W. Mao et al., "A flexible electrode array for determining regions of motor function activated by epidural spinal cord stimulation in rats with spinal cord injury," *Neural Regener. Res.*, vol. 17, no. 3, pp. 601–607, Mar. 2022.

[26] H.-P. Wang et al., "A wireless wearable surface functional electrical stimulator," *Int. J. Electron.*, vol. 104, no. 9, pp. 1514–1526, Sep. 2017.

[27] N. R. Council, *Guide for the Care and Use of Laboratory Animals*, 8th ed. Washington, DC, USA: The National Academies Press, 2011, p. 246.

[28] J. F. S. Vieira, C. Shieff, B. S. Nashold Jr., D. E. Bullard, and E. Cosman, "Impedance measurements of the spinal cord of man and animals," *Stereotactic Funct. Neurosurgery*, vol. 51, nos. 2–5, pp. 154–163, 1988.

[29] R. M. Ichiyama, Y. P. Gerasimenko, H. Zhong, R. R. Roy, and V. R. Edgerton, "Hindlimb stepping movements in complete spinal rats induced by epidural spinal cord stimulation," *Neurosci. Lett.*, vol. 383, no. 3, pp. 339–344, Aug. 2005.

[30] J. M. Akers, P. H. Peckham, M. W. Keith, and K. Merritt, "Tissue response to chronically stimulated implanted epimysial and intramuscular electrodes," *IEEE Trans. Rehabil. Eng.*, vol. 5, no. 2, pp. 207–220, Jun. 1997.

[31] J. T. Hachmann et al., "Large animal model for development of functional restoration paradigms using epidural and intraspinal stimulation," *PLoS ONE*, vol. 8, no. 12, Dec. 2013, Art. no. e81443.

[32] M. S. Heo, H. S. Moon, H. C. Kim, H. W. Park, Y. H. Lim, and S. H. Paek, "Fully implantable deep brain stimulation system with wireless power transmission for long-term use in rodent models of Parkinson's disease," *J. Korean Neurosurgical Soc.*, vol. 57, no. 3, pp. 152–158, Mar. 2015.

[33] C. Gautam, J. Joyner, A. Gautam, J. Rao, and R. Vajtai, "Zirconia based dental ceramics: Structure, mechanical properties, biocompatibility and applications," *Dalton Trans.*, vol. 45, no. 48, pp. 19194–19215, 2016.

[34] P. Musienko et al., "Somatosensory control of balance during locomotion in decerebrated cat," *J. Neurophysiol.*, vol. 107, no. 8, pp. 2072–2082, 2012.

[35] J. Zhang et al., "Inhibiting spasticity by blocking nerve signal conduction in rats with spinal cord transection," *IEEE Trans. Neural Syst. Rehabil. Eng.*, vol. 29, pp. 2355–2364, 2021.

[36] Y. Zhou, S. Ma, Z. G. Wang, H. Zhang, and K. Wang, "Analysis and design of high-efficiency charge pumps with improved current driving capability using gate voltage boosting technique," *IEEE Trans. Circuits Syst. I, Reg. Papers*, vol. 69, no. 6, pp. 2364–2375, Jun. 2022.

[37] Z.-G. Wang et al., "Microelectronic channel bridge and signal regeneration of injured spinal cords," in *Proc. IEEE Asia Pacific Conf. Circuits Syst.*, Nov. 2008, pp. 658–661.

[38] Z. Wang et al., "Microelectronics-embedded channel bridging and signal regeneration of injured spinal cords," *Prog. Natural Sci.*, vol. 19, no. 10, pp. 1261–1269, Oct. 2009.

[39] Z. Wang, X. Gu, and X. Lü, "Neural channel bridge aided by a microelectronic system," U.S. Patent 8 000 806 B2, 2011.

[40] Z. Huang et al., "The principle of the micro-electronic neural bridge and a prototype system design," *IEEE Trans. Neural Syst. Rehabil. Eng.*, vol. 24, no. 1, pp. 180–191, Jan. 2016.